communications earth & environment

Article

https://doi.org/10.1038/s43247-024-01455-y

Event-specific ground motion anomalies highlight the preparatory phase of earthquakes during the 2016–2017 Italian seismicity

Check for updates

Matteo Picozzi[1] ✉, Daniele Spallarossa[2], Antonio Giovanni Iaccarino[3] & Dino Bindi[4]

Although physical models are improving our understanding of the crustal processes that lead to large earthquakes, observing their preparatory phases is still challenging. We show that the spatio-temporal evolution of the ground motion of small magnitude earthquakes can shed light on the preparatory phase of three main earthquakes that occurred in central Italy between 2016 and 2017. We analyze systematic deviations of peak ground accelerations generated by each earthquake from the values predicted by a reference ground motion model calibrated for background seismicity and refer to such deviations as event-specific ground motion anomalies (eGMAs). The eGMA temporal behavior indicates that during the activation phase of the main earthquakes, the ground shaking level deviates, positively or negatively, from the values expected for the background seismicity. eGMA can be exploited as beacons of stress change and help to monitor the mechanical state of the crust and the nucleation of large earthquakes.

Due to the complex nature of the Earth's crustal processes and the impossibility of observing rupture phenomena directly at the fault surface, earthquake generation remains an unresolved fundamental scientific question[1]. Small size seismic events occurring before a large earthquake (foreshocks)[2] are considered hints for preparatory processes occurring within a nucleation region. Foreshocks became one of the most studied precursors[3–6], but over the years the researchers' enthusiasm about them has waned, mainly because they have not been systematically observed. In fact, the occurrence of foreshocks is related to an unpredictable combination of heterogeneous fault properties, stress interactions and crustal fluids, which it may also explain why nearby faults show in many areas, such as in central Italy, show different precursory patterns. Recently, it has been proposed that the generation of large earthquakes is related to a progressive localization of shear deformation around a rupture zone[7]. This process progressively evolves into a rapid final loading of a crustal volume where the major dynamic rupture occurs, but the final triggering hypocenter position remains stochastic[8]. Similar patterns of damage evolution are also observed by acoustic emissions during triaxial tests on rock samples[9], suggesting that the process generating earthquakes may be universal. Laboratory experiments also suggest that both the spatio-temporal evolution and source properties of acoustic emissions provide valuable information for intercepting the rupture preparation process[10,11].

Unfortunately, crucial information for a better understanding of the preparatory process of large earthquakes, such as the source parameters stress drop and seismic energy, are subject to large uncertainties and are difficult to obtain for small magnitude earthquakes[12]. For this reason, following previous studies[13–15], here we revisit the preparatory phase of three large-magnitude earthquakes that occurred during the complex multiple mainshocks sequence in central Italy between 2016 and 2017 by studying the spatio-temporal evolution of event-specific ground motion anomalies (eGMAs) estimated for the peak ground acceleration (PGA).

We recall that eGMA is a concept originally developed within the seismic hazard community to describe ground motion residuals associated with repeated source effects that are not captured by the magnitude and distance scaling in the ground motion reference model[16]. In other words, eGMA provides information on the ground motion intensity variability associated with source processes other than those considered in the calibration of the reference ground motion model, GMM. For this reason, eGMA absorbs the variability of several source parameters, such as stress drop, source frictional properties and source volume rheology[17,18].

For a more intuitive understanding of the eGMA concept, we can imagine the occurrence of two earthquakes of the same magnitude but with different stress drop, $\Delta\sigma$, for example due to the presence of crustal fluids

[1]National Institute of Oceanography and Applied Geophysics – OGS, Trieste, Italy. [2]DISTAV, University of Genoa, Genoa, Italy. [3]University of Naples Federico II, Naples, Italy. [4]Helmholtz Centre Potsdam, GFZ German Research Centre for Geosciences, Potsdam, Germany. ✉e-mail: mpicozzi@ogs.it

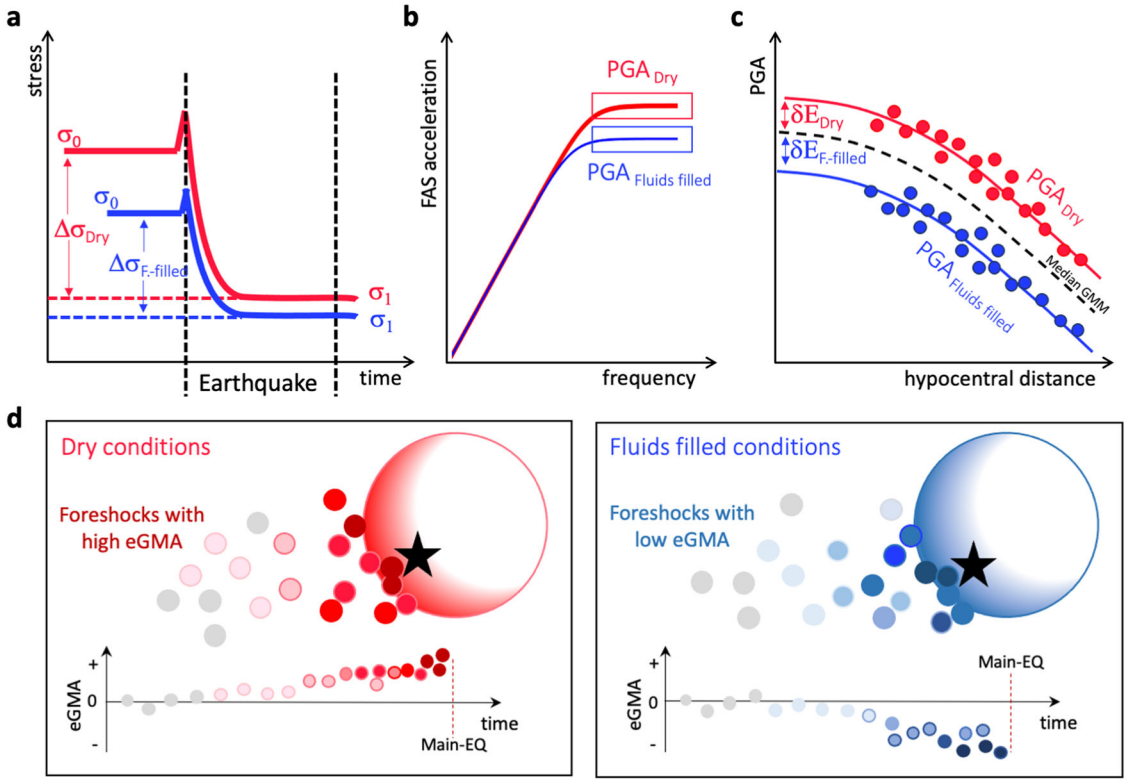

Fig. 1 | Schematic illustrations of the eGMA concept and of two end-member preparation models. a Temporal evolution of stress for ruptures occurring in dry (red) and fluid filled (blue) conditions, earthquake 1 (Eq1) and 2 (Eq2), respectively. Initial stress, σ_0, final stress, σ_1, stress drop ($\Delta\sigma = \sigma_0 - \sigma_1$) in dry, $\Delta\sigma_{Dry}$, and fluid filled conditions, $\Delta\sigma_{F.-filled}$. **b** Fourier Amplitude Spectra, FAS, in acceleration for the Brune source model[55] considering the same seismic moment, but $\Delta\sigma_{Dry}$ (red, Eq1) and $\Delta\sigma_{F.-filled}$ (blue, Eq2). The two boxes highlight the region of the source spectra from which the peak ground acceleration has origin. **c** Representation of the δE concept eGMA. Median ground motion model calibrated on background seismicity (black dashed line), PGA from recordings associated to Eq1 (red dots) and Eq2 (blue dots), median for the two earthquakes (blue and red lines for Eq1 and Eq2, respectively). **d** The two panels show the earthquake preparation with foreshock activity associated to high eGMA (high stress drop, $\Delta\sigma_{Dry}$, left panel) and low eGMA (low stress drop, $\Delta\sigma_{F.-filled}$, right panel). Within the two panels it is outlined the eGMA temporal pattern for earthquakes during the preparation phase.

(Fig. 1a)[19]. The resulting acceleration source spectra for these hypothetical earthquakes will be characterized by different high frequency plateau levels (Fig. 1b), which in turn will result in PGA values for the two events systematically above (high Δσ) or below (low Δσ) the median GMM (Fig. 1c). The resulting average deviation of the PGA values for an event from the GMM is the eGMA (computed as event-specific residuals). As is often the case, a method developed for one scientific purpose also proves useful for other applications. Recently, eGMA has also been used for investigating fault healing[20], the preparation phase of earthquake nucleation[21–23], the spatio-temporal evolution of reservoir-induced seismicity[15], and for on-site early warning applications[24,25]. For our purpose, we refer to a simple model[26] that allows us to consider the parameter eGMA as a proxy for the relative crustal stress conditions at the source hypocenter (see Methods). Therefore, positive and negative eGMA values for small earthquakes observed before a larger one can be intuitively interpreted as a collective behavior of the small seismicity in response to an excess or deficit of crustal stress conditions anticipating a larger rupture process.

Our aim is to test whether the ground motion characteristics of the small earthquakes occurring during the preparation phase of the mainshocks show anomalous patterns with respect to those expected for the background seismicity (as in the two examples of Fig. 1d). To this end, we calibrate a reference ground motion model (GMM) for the PGA using the background seismicity (i.e., removing clustered events) that occurred during the period 2011–2015. We use the GMM predictions to monitor the temporal evolution of the eGMA.

We focus our analysis on the 2016–17 seismic sequence that occurred in central Italy. As the first mainshock of the sequence, i.e., the Mw 6.0, 24 August 2016 Amatrice earthquake (AMA16), was anticipated by a long-lasting quiescence[27], we consider here as target events: the Mw 6.1, 26 October 2016 Visso earthquake (VIS16), the Mw 6.5, 30 October 2016 Norcia earthquakes (NOR16), and the Mw 5.4, 18 January 2017 Capitignano earthquake (CAP17).

Our seismic catalog, derived from a fully automated and robust processing strategy [28], consists of 61226 earthquakes recorded between 2006 and 2023 with magnitudes ranging from Mw 1.5 to Mw 6.5, while hypocentral depths vary between 1 km and 20 km (Fig. 2 and Supplementary Fig. 1).

We show that eGMA allows tracking the spatio-temporal evolution of the preparation phase for VIS16, NOR16 and CAP17. Our results indicate that the small earthquakes that occur during the activation phase, in the region where large earthquakes nucleate, have a peculiar imprint with respect to the background earthquakes and carry information about the preparatory process of the large earthquakes. Although the final activation may have different characteristics, the relevance of our results lies in the fact that the ability to detect deviations of the ground shaking from the background level could help in the future to identify small earthquake sequences that are prone to evolve into catastrophic sequences.

Results

Spatio-temporal evolution of event-specific ground motion anomaly

The Apennines orogen had a multiphase evolution, which led to shallower high angle normal faults to penetrate with deeper sub-horizontal detachment faults[29]. The interaction of seismicity on the normal and detachment faults was considered to play a considerable role in the preparation and evolution of the 2016–2017 seismic sequence[30]. For this reason, we first look at the spatial distribution of eGMAs in the periods preceding the three

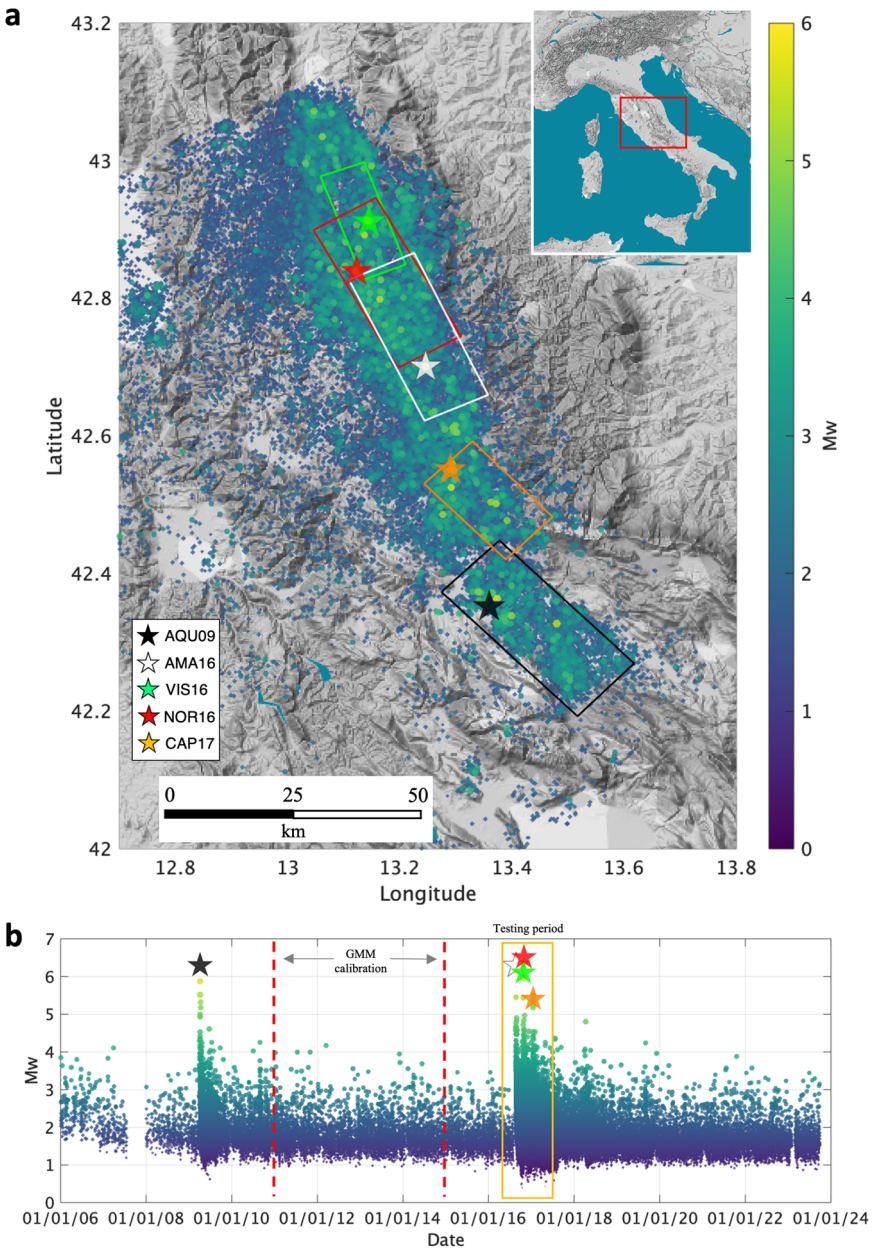

Fig. 2 | Seismic events occurred in central Italy during the period 2006–2023. a Distribution of earthquakes (dots colored per magnitude). The five main earthquakes are indicated by colored stars (AQU09 black, AMA16 white, VIS16 green, NOR16 red, and CAP17 orange). The rectangles depict the surface projection of the faults of the mainshocks[58,59]. **b** Distribution of events magnitude in time. The events occurred in the period 2011–2025 (between the dashed vertical lines) have been used to calibrate the ground motion model (Eq. (1)).

mainshocks studied, and for each event we group the earthquakes according to their hypocentral depth (i.e., above or below 6 km, which is considered a reasonable depth to separate the contribution of normal and detachment faults; hypocentral depths of the events are shown in Supplementary Fig. 1).

VIS16, whose observing period starts shortly after AMA16, shows relatively low eGMA values for shallow earthquakes (Fig. 3a) and high values for earthquakes deeper than 6 km (Fig. 3b). In the following, we will discuss the relation between eGMA and stress. According to this relation, the eGMA differences shown in Fig. 3 can be interpreted in relation to the increase of crustal stress with depth. The shallower and deeper seismicity also shows distinct eGMA values for NOR16 and CAP17. We find interesting the high GMA patch on the south-eastern edge of which NOR16 has nucleated (Fig. 3d). The latter coincides with a high apparent stress patch[31] affected by a positive Coulomb stress change after the two previous mainshocks of the sequence[32]. The seismicity preceding CAP17 also shows a peculiar pattern, with no activity in the considered shallow layer and seismicity characterized by high eGMAs in the deep layer (Fig. 3e, f).

An overview of the spatio-temporal evolution of eGMA for the three investigated periods can be seen in Fig. 4. Considering VIS16 (Fig. 4a), we observe that, when we keep as reference the along the strike distance between AMA16 and VIS16 (blue dashed line), the seismicity progressively migrate towards the VIS16 epicenter and eGMA increases. The asymmetric distribution of either the earthquakes and their eGMAs also applies to NOR16 and CAP17. Of note is the sudden increase in eGMAs a few hours before VIS16 and CAP17 (see the temporal zoom in Fig. 4d, f), and a sequence of events a few kilometers south of NOR16 with initially higher and later lower eGMAs (Fig. 4e).

The peculiar spatio-temporal evolution of both hypocenters and eGMA values, motivated us to further investigate eGMA during the considered preparatory phases. We therefore examine their daily cumulation over time (ΣeGMA), and for homogeneity we consider the last four days before the three mainshocks. Taking each of the three mainshocks as reference, we split the small earthquakes preceding them into two subsets according to their location with respect to the mainshock. We consider their positive or negative hypocentral distance, projected along the Apennines strike, from the main event (the corresponding eGMAs are shown in Supplementary Figs. 2–4, with panels showing the earthquakes per days before the mainshocks). ΣeGMA is computed cumulating eGMA values

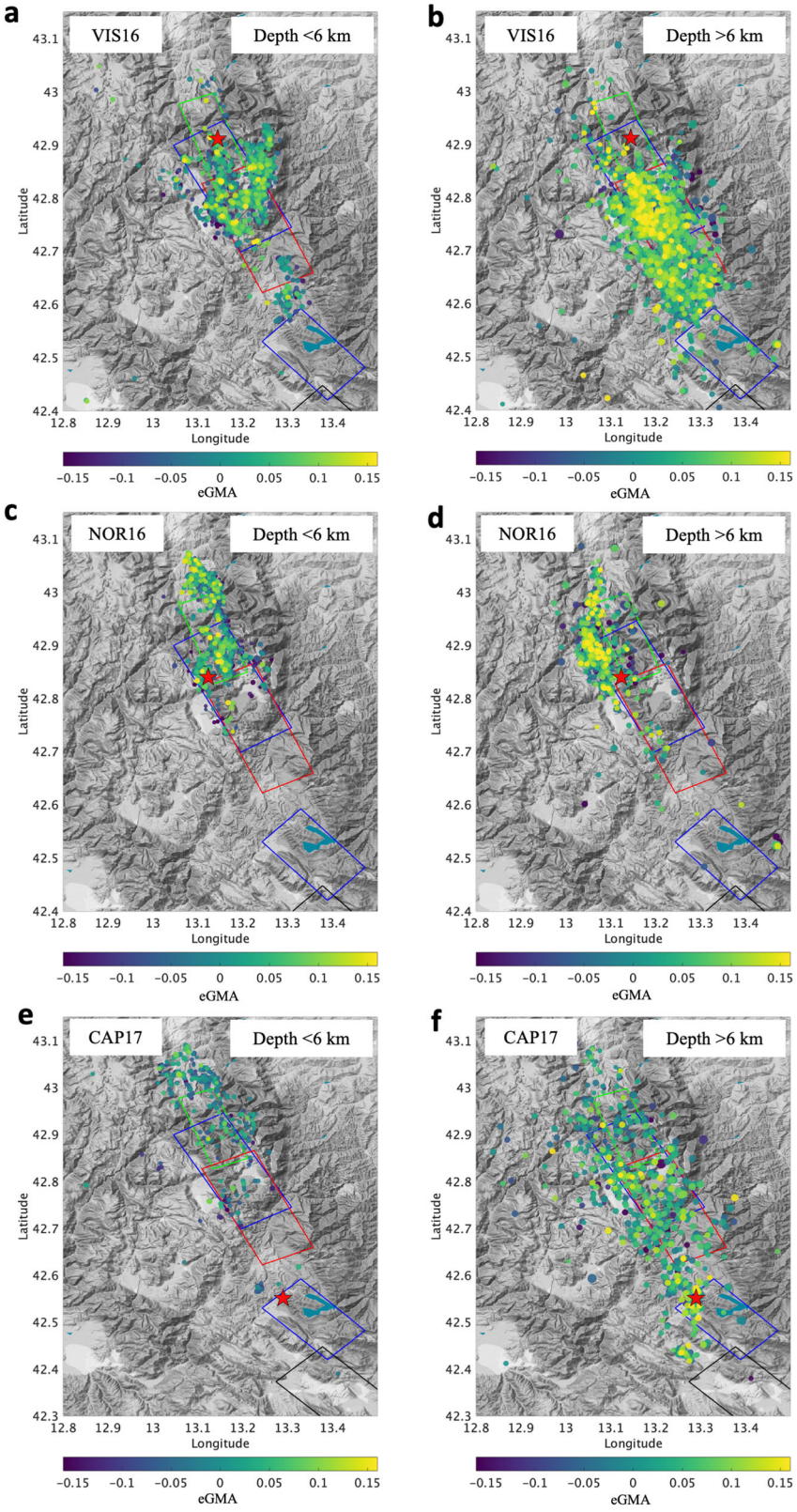

Fig. 3 | Distribution small magnitude events colored per eGMA. The events are split according to hypocentral depth, preceding the three main earthquakes considered in this study. **a** Seismicity preceding VIS16 (red stars) and hypocentral depth smaller than 6 km. The events are colored per eGMA. The surface projection of the main faults[58,59] are shown. **b** The same as **a**, but for seismicity deeper than 6 km. **c** and **d** the same as **a** and **b**, respectively, but for NOR16. **e** and **f** the same as **a** and **b**, respectively, but for CAP17.

starting from Southeast and from Northwest, respectively, considering thus first the more distant events and then moving towards the mainshock (Fig. 5, with data colored per day before the mainshock). Looking at VIS16, we see ΣeGMA increasing during the last day before the main event (Fig. 5a). A similar behavior is seen for CAP17 too (Fig. 5c). We can thus interpret VIS16 and CAP17 as related to the increase in stress before the main rupture. Worth to note, the observed trends are considerably larger than the uncertainty on ΣeGMA.

Conversely, during the preparation phase of NOR16, we see ΣeGMA to vary asymmetrically, with the northwestern sector of the fault being interested by high spatio-temporal changes, and strong temporal variation (Fig. 5b). We find particularly intriguing the ΣeGMA change from positive

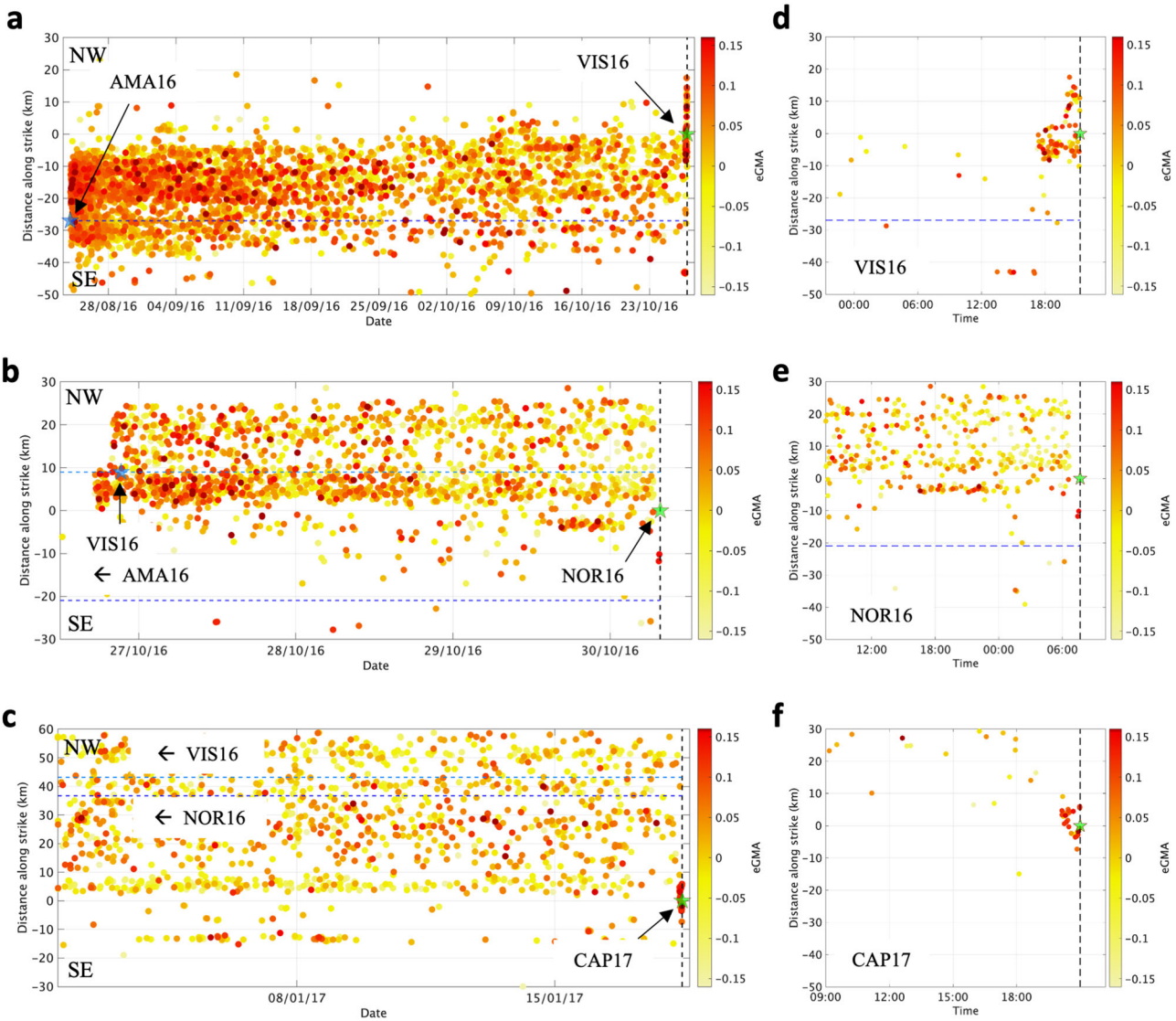

Fig. 4 | Spatio-temporal distribution of small magnitude events colored per eGMA. The events are preceding the mainshocks of **a** VIS16, **b** NOR16, and **c** CAP17. The temporal zoom for VIS16, NOR16, and CAP17 is shown in **d**, **e**, and **f**, respectively.

to negative values. NOR16 seems, in fact, anticipated by an initial condition of high crustal stress level that progressively decreases during the considered period. The eGMA decrease agrees with the previously observed reduction in seismic radiated energy [31]. The preparatory mechanism seen for NOR16 by eGMA agrees with previous Coulomb stress change modeling[32] that hypothesized a stress decrease in the hypocentral crustal volume being related to pore pressure increase caused by fluid flow in the upper crust. Crustal fluids are thus considered responsible for a stress corrosion mechanism that led to a clock advance for the Norcia earthquake[32] and eGMA allows to follow the spatio-temporal evolution of this process.

We now consider the link between eGMA and crustal earthquake source parameters[26], and we explicitly express the link between eGMA variations and those in static stress drop, $\Delta\sigma$, with respect to the average $\Delta\sigma$ value for the earthquakes used calibrating the GMM (see Method).

Modeling the spatio-temporal evolution of eGMA in terms of $\Delta\sigma$ variations, and considering the small earthquakes as beacons of stress, allows us to achieve a first order estimate of the stress changes occurred in the mainshock hypocenter volume during the days preceding the main rupture. To highlight the spatio-temporal stress changes, we calculate the derivative of the stress variation with the hypocentral distance, D, along the strike direction, $\delta\Delta\sigma/\delta D$ (Fig. 6, while the corresponding stress variations are shown in Supplementary Figs. 5–7). We consider bins 5 km wide, and we estimate the relevant uncertainty with a Monte Carlo approach (Fig. 6, see Method). This change of perspective from eGMA to the along strike gradient of $\Delta\sigma$ suggests for NOR16 a progressive decrease in stress drop of almost one order of magnitude during the last day and approaching the mainshock hypocenter (brown curve, Fig. 6b), and of almost three orders of magnitude if we consider the stress variation during the last four days at the closest distance to the mainshock hypocenter (from yellow to brown stars, Fig. 6b). Conversely, for both VIS16 and CAP17, we observe that approaching the mainshock hypocenter and during the day before the main events the stress almost tripled (Fig. 6a, c). For these earthquakes, we also computed the evolution of $\delta\Delta\sigma/\delta D$ considering one month before the mainshocks (Supplementary Fig. S8, where the results for the last day before the mainshock are shown in red and those for the previous 29 days are in gray). Even these results confirm that for both VIS16 and CAP17 the activation phase started during the last day before the mainshocks.

Discussion

The spatio-temporal evolution of small magnitude earthquakes unveiled the progressive crustal weakening process occurred in central Italy after the 2009 L'Aquila earthquake[30,33,34]. It is in fact hypothesized that the pluri-annual activity of the basal detachment faults leads to the progressive unlocking of the overlying normal faults, in agreement with the progressive deformation localization model proposed by Ben-Zion and Zaliapin[8]. In this

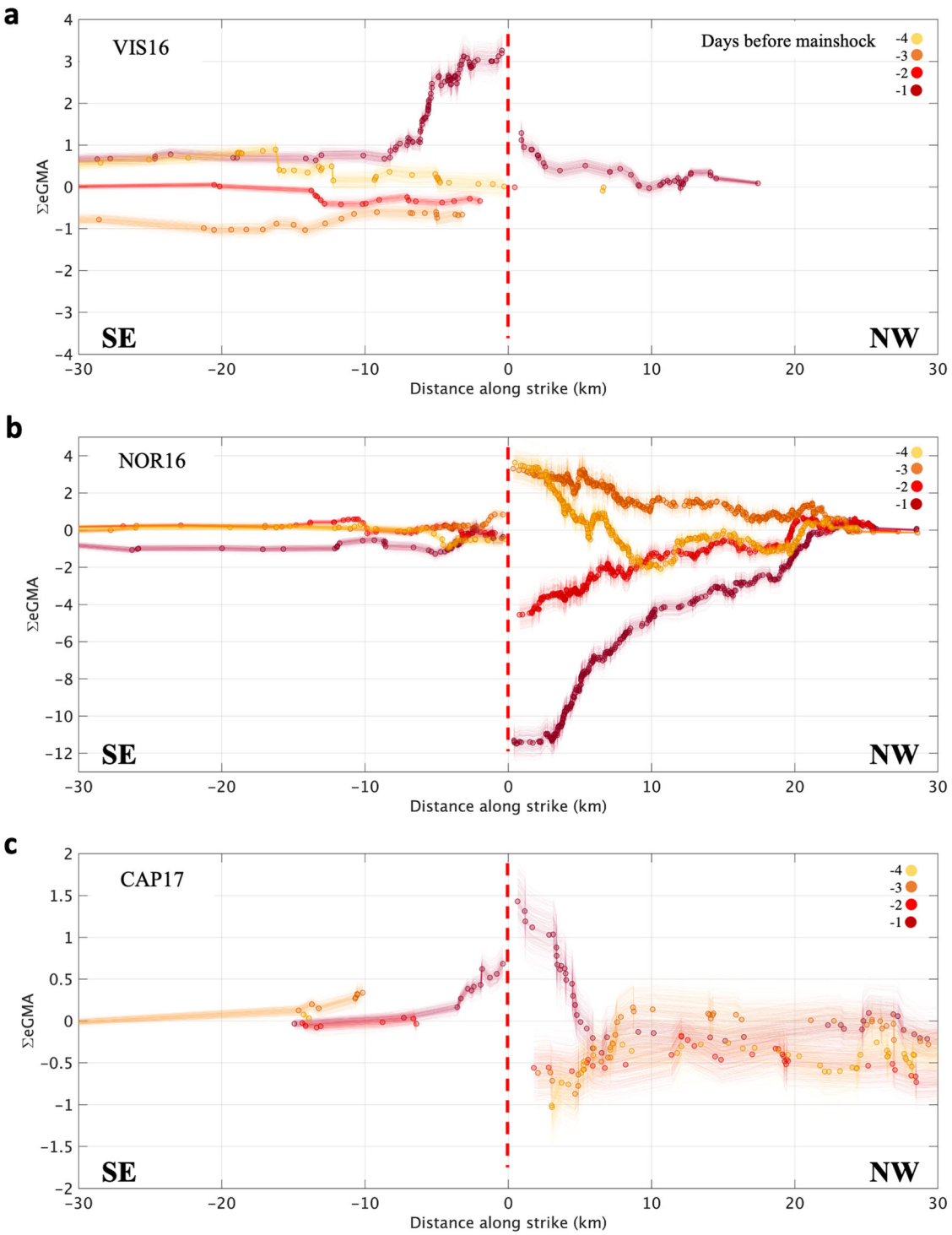

Fig. 5 | ΣeGMA computed for different days. The events are preceding the mainshocks of preceding **a** VIS16, **b** NOR16, and **c** CAP17 (from −4 days, yellow, to −1 day, dark red). The uncertainty associated to ΣeGMA is computed by a bootstrap approach[50] and represented as colored lines (see Method).

framework, the event-specific ground motion anomalies for small earthquakes provide a complementary information, playing as beacons of crustal stress and its spatio-temporal evolution.

The progressive migration of seismicity between AMA16 and VIS16 seen by eGMA indicates a progressive change in the earthquakes' dynamic characteristics, especially during the final activation of VIS16. The eGMA increase suggests an increase of the stress conditions under which the small earthquakes occur. A similar behavior is also observed for the period between NOR16 and CAP17, with the latter event also anticipated by an eGMA increase during the last few hours preceding the main rupture.

It is widely discussed what causes large earthquakes in central Italy. While they are likely driven by slow slips episodes[33,34], it is not clear yet how the latter interplay during a seismic sequence with post-seismic deformation and subsequent faults loading. Even crustal fluids might have played a crucial role in the preparation phase of the 2016–2017 central Italy earthquakes[35].

The different precursor patterns observed for AMA16, which was preceded by quiescence, VIS16 and CAP17 compared to NOR16 and AQU09 show as different precursory paths before a large earthquake are possible due to the stress accumulation on the faults[36], which in turn can be influenced by the interaction of multiple factors, such as different

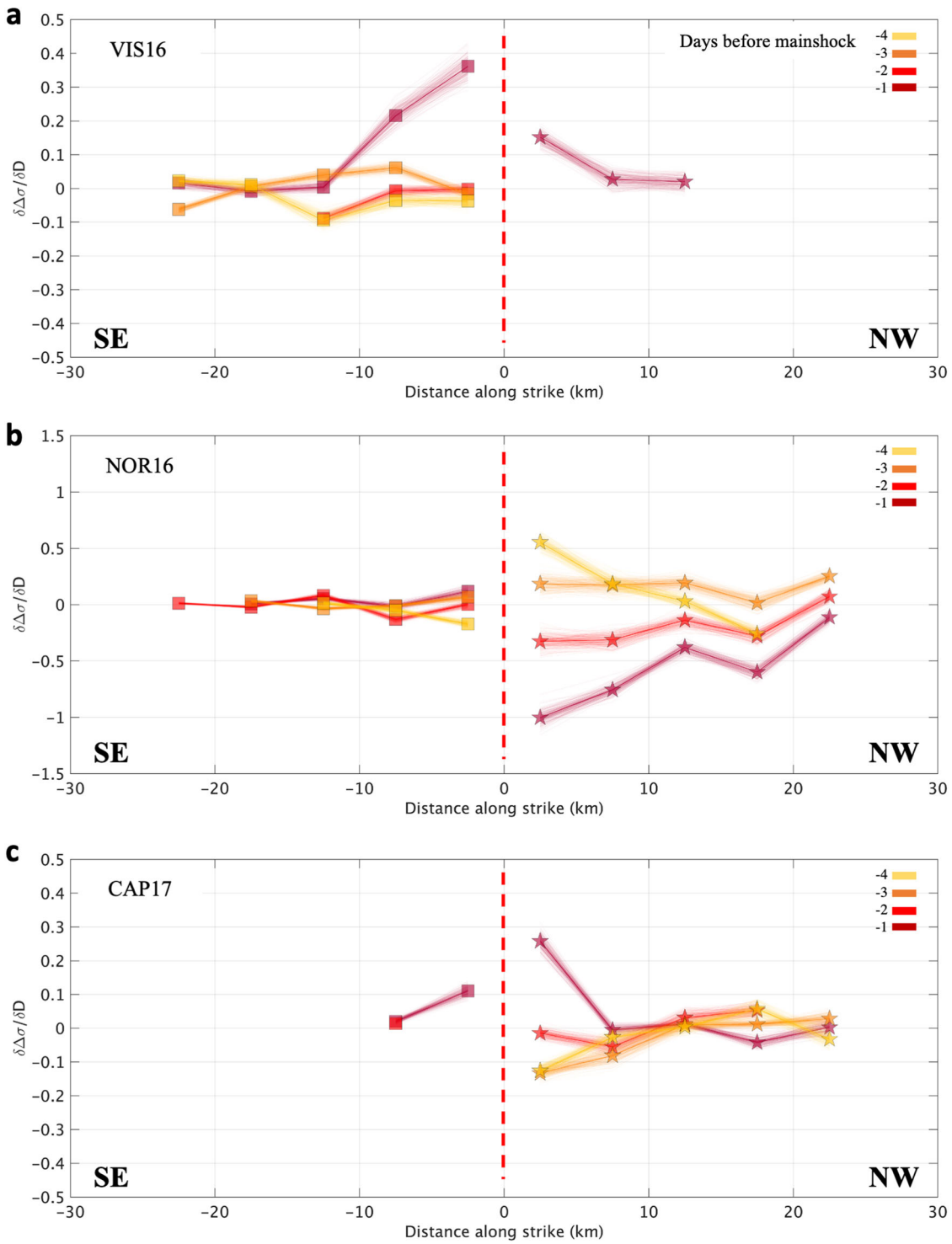

Fig. 6 | Stress change with hypocentral distance along the strike direction. The same as Fig. 5, with **a** VIS16, **b** NOR16, and **c** CAP17, but showing δΔσ/δD (squares and stars for earthquakes occurred south and north of the mainshock, respectively). The uncertainty associated to δΔσ/δD is computed by a bootstrap approach[53] and represented as colored lines (see Method).

heterogeneous fault properties, stress interactions, and crustal fluids. eGMA indicates that the stress conditions under which large earthquakes nucleate can be highly variable, explaining us why systematic precursory patterns during the generating large earthquakes are not found and the background physical processes of the earthquake nucleation are not fully understood yet.

Likely, systematic studies of more test cases considering the spatio-temporal evolution of different source parameters in different tectonic context might help to identify systematic patterns in the preparatory phase of large earthquakes. In our study, eGMA highlights similarities between VIS16 and CAP17. We can also tentatively interpret our results according to the Cattania and Segall[37] modeling. For VIS16 and CAP17, foreshocks likely occurred at the boundary of a large asperities with high normal stress (high eGMA, Fig. 1d left panel). Foreshocks might thus play a crucial role in the main rupture occurrence by increasing the asperity' stress level and shrinking the nucleation length, promoting the occurrence of the destructive event[37]. The peculiar behavior observed for the NOR16 preparatory phase is likely related to the

presence of crustal fluids, which, as anticipated above, might have contributed to decrease the normal stress in the hypocentral volume[32] (low eGMA, Fig. 1d right panel), and the interaction of faults involved in the 2016–2017 central Italy seismic sequence[31]. High-pressure, deep, CO_2-dominated fluids were considered responsible for the nucleation of also previous large earthquakes along the central and southern Apennines (e.g., the 1997 Colfiorito, the 2009 L'Aquila, and the 2016 seismic sequences)[38–41]. It is worth noting that a trend in eGMA like the one of NOR16 is observed also for the 2009, Mw 6.1L'Aquila earthquake (Supplementary Fig. 9). Despite for this latter event only 54 earthquakes with magnitude between Mw 1.5 and Mw 3.5 are available from the 30 March 2009 to the 6 April 2009), we observe that the temporal evolution of eGMA and ΣeGMA agree with the sudden decrease in the apparent stress observed during the preparatory phase[42].

Regardless of which factor was predominant in promoting the studied large earthquakes, our results indicate that monitoring the spatio-temporal evolution of eGMA can provide useful information about the preparatory phase of large earthquakes, highlighting deviations from the normal behavior of background seismicity. Although based on simple assumptions, the model[26] used to link eGMA to stress drop allows us to interpret the ground motion anomalies as excess or deficit in crustal stress, to figure out the stress spatio-temporal variations around a rupture zone and to follow the evolution of the earthquake preparation phases. Our eGMA study falls thus into the idea of exploiting microearthquakes as beacons of stress for the mechanical state of the crust[31,42]. Future studies will be directed to investigate if eGMA can allow improving our understanding of the nucleation of large earthquakes and strong aftershocks[43].

Methods

Data and preliminary analyses

We estimate peak ground acceleration, PGA, and event parameters (moment magnitude and location) exploiting a consolidated procedure developed by the research group at the University of Genoa, Italy. We use the service RAMONES[28] to extract and analyze segments from continuous data streams stored in the ORFEUS-EIDA (https://www.orfeus-eu.org/data/eida/), IRIS and DPC (http://ran.protezionecivile.it/EN/index.php) repositories. We used data mainly from networks IV (DOI: 10.13127/SD/X0FXnH7QfY), IT (DOI: 10.7914/SN/IT) and MN (https://doi.org/10.13127/SD/fBBBtDtd6q).

Then, we follow automatic procedures[44–46], where P and S waves onsets are detected, the event locations and local magnitudes are estimated, and the waveforms feature related to M_0 is extracted from recordings. Uncertainties in event location are mostly within 1 km both horizontally and vertically. Using empirical attenuation models calibrated for a wide region of the central Apennines (Italy)[28] (i.e., within a region bounded by 40.0°N and 44.5°N in latitude and 10.50°E and 16.50°E in longitude), we estimate M_0 for earthquakes with magnitude above Mw 1.5. For the sake of simplicity, we refer to Spallarossa et al.[28] for more details on the procedure for estimating M_0 and for a validation of the results.

Event-specific Ground Motion Anomaly computation

The event-specific ground motion anomaly (eGMA) is related to the concept of residuals between observed and predicted values for a selected ground motion parameter. For each earthquake, the eGMA is evaluated by comparing the peak ground acceleration (PGA) values recorded at several stations with the predictions from a reference ground motion model (GMM, Fig. 1c). Therefore, following previous applications in the southern Apennines[13–15], we first calibrate a regional GMM by performing a mixed-effects regression[47,48] on the model:

$$\log(\mathrm{PGA}) = e1 + e2\cdot(M - M_{\mathrm{ref}}) + e3\cdot(M - M_{\mathrm{ref}})^2 + e4\cdot\log(R_{\mathrm{hypo}}) + e5\cdot R_{\mathrm{hypo}} + e6\cdot D_{\mathrm{hypo}} + \delta\mathrm{E} + \delta\mathrm{S} + \varepsilon \quad (1)$$

where PGA (in m/s^2) is computed as the root mean square (RMS) of the values recorded over the two horizontal components; M is the moment magnitude; M_{ref} is the reference magnitude (set to 1.5 according to Picozzi et al.[31]); Rhypo and Dhypo are the hypocentral distance and depth, respectively.

With respect to previous GMM calibrated for monitoring microseismicity[13–15], we introduce in Eq. (1) an explicit dependence of the predictions on the hypocentral depth. The model coefficients $e1$ to $e6$ define the mean PGA predicted for each combination of the explanatory variables: magnitude, distance, and depth. The introduction of the random effects δE and δS allows the distribution of the residuals ξ, computed as the difference between the observed PGAs and the mean predictions, to be partitioned into event-specific and station-specific contributions, respectively, while all remaining contributions are absorbed by the left-over distribution ε. In the context of seismic hazard studies, δE and δS are referred to as between-event and between-station residuals[16]. By construction, δE, δS and ε approximate zero-mean normal distributions with standard deviations τ, ϕ_S and ϕ_0, respectively; since δE, δS and ε are independent distributions, the standard deviation σ of the whole residual distribution ξ is given by $(\tau^2 + \phi_S{}^2 + \phi_0{}^2)^{0.5}$. The data set used to calibrate the reference GMM consists of events that occurred between 2011 and 2015, a period in which no events with Mw >4.5 occurred. To remove the presence of clusters, we perform a cluster analysis[49] to identify the background seismicity that is used to calibrate the GMM. The selected data set consists of 1793 earthquakes with Mw between 1.5 and 3.4, and hypocentral depths up to 25 km; considering Rhypo < 100 km, the reference GMM in Eq. (1) is calibrated using 40657 PGA values recorded by 138 seismic stations. To avoid possible biases due to the conversion among different magnitude scales[20,50], the moment magnitudes are derived uniformly according to the RAMONES procedure[28].

Results of model (1) calibration are summarized in Supplementary Table S1 and Supplementary Fig. 10. The obtained δE well approximates a zero-mean normal distribution (Supplementary Fig. 10b), and the values for the different earthquakes do not show pronounced trends with hypocentral depth (Supplementary Fig. 10c). Furthermore, both the total residuals ξ and the left-over residuals ε show no bias with respect to both hypocentral distance and depth (Supplementary Fig. 10d–g).

Equation (1) considers only moment magnitude[28] and hypocentral depth as source parameters controlling the ground shaking. Since other kinematic or dynamic source characteristics may contribute to the shaking level, δE captures the event-specific PGA variability generated by differences between earthquakes in these unaccounted source parameters. Therefore, δE represents the eGMA of the earthquakes included in the calibration data set. We are interested in extending the concept of eGMA to new earthquakes not included in the calibration dataset, considering periods of different durations preceding the three analyzed mainshocks (see Supplementary Table S2 for information on the considered period, the number of earthquakes, stations, and ground motion data for each series of earthquakes preceding the three mainshocks). For this purpose, we follow Kotha et al.[51,52] by computing

$$eGMA = \frac{\tau^2\sum_{s=1}^{n_e}(\log(PGA)_{e,s} - \log(\mu_{e,s}))}{n_e\tau^2 + \phi^2} \quad (2)$$

where n_e is the number of available recordings for event e; $PGA_{e,s}$ is the observed ground motion for event e recorded at station s; $\mu_{e,s}$ is the corresponding predicted mean value; $\phi=(\phi_S{}^2 + \phi_0{}^2)^{0.5}$ is the so-called within-event standard deviation (i.e., equal to 0.47) and τ the δE standard deviations (i.e., 0.08). As explained in the maintext, ΣeGMA is computed as the cumulative of eGMA. The uncertainty on eGMA and ΣeGMA is computed through a bootstrap approach[53] by considering 200 realizations of a random sampling with replacement.

Event-specific Ground Motion Anomaly and relation to stress

We relate PGA to the seismic moment (M_0) and stress drop (Δσ) through the following model[26]

$$PGA = 3.3M_o^{\frac{1}{3}}\Delta\sigma^{\frac{2}{3}}\frac{\beta_A}{R\sqrt{\kappa\left[\frac{1}{kC_S}\right]\left(\frac{7M_o}{16\Delta\sigma}\right)^{\frac{1}{3}} + \frac{R}{C_S}\left[1 + 1.5^{\frac{-1}{4}}\pi\kappa kC_S\left(\frac{16\Delta\sigma}{7M_o}\right)^{\frac{1}{3}}\right]^2}} \quad (3)$$

where, κ is the anelastic and near surface attenuations parameter (Anderson and Hough[54]), C_S is the S wave velocity, R is the hypocentral distance, k is a constant as function of the adopted source model and rupture velocity (Brune[55]; Madariaga[56]), and β_A includes the influence of parameters related to density, free surface effects, radiation pattern and S-wave velocity (see Lior and Ziv [26]).

We use a Monte Carlo like approach to generate the synthetic catalog of eGMA values. We assume that $\Delta\sigma$ is normally distributed (mean $\Delta\sigma$ equal to 1 MPa, Supplementary Fig. 11a). Further, we assume that the seismicity follows a simple a Gutenberg-Richter distribution[57] (b value equal to 1, Supplementary Fig. 11b). We only select earthquakes in the range of magnitudes between Mw 1.5 and Mw 3.4 as for the experimental dataset, which corresponds to ~16,500 earthquakes. For each earthquake (characterized by a seismic moment derived by the moment magnitude), we extract a random value of $\Delta\sigma$ from the stress drop distribution. Then, we randomly extract 50 hypocentral distances, R, from a uniform distribution bounded at 5 km and 50 km. This set of information (M_0, the random $\Delta\sigma$, $\Delta\sigma_i$, and the fifty hypocentral distances) is used in Eq. (3) to compute synthetic PGA values (PGA_i). Similarly, we consider the same M_0 and the fifty hypocentral distances as above, but the median $\Delta\sigma$ (the reference $\Delta\sigma_r$), to compute by Eq. (3) the PGA values for the median GMM (PGA_m). The average of differences between PGA_i and PGA_m values is the event-specific PGA variability, eGMA. Then, we relate the eGMA values with the logarithm of the $\Delta\sigma_i$ over $\Delta\sigma_r$ ratio $[\delta\Delta\sigma = \log(\Delta\sigma_i/\Delta\sigma_r)]$ (Supplementary Fig. 11c).

We perform a linear regression between eGMA and $\delta\Delta\sigma$ (Supplementary Fig. S10c) obtaining the following relation:

$$\delta\Delta\sigma = 1.370(\pm 0.001) \cdot \mathrm{eGMA} + 0.00045(\pm 0.00002) \quad (4)$$

Equation (4) is thus used to estimate $\delta\Delta\sigma$ considering eGMA from real data. As discussed, $\delta\Delta\sigma$ is then used to compute the derivative of the stress change with respect to the hypocentral distance along the strike direction, $\delta\Delta\sigma/\delta D$. As done for eGMA, the uncertainty of $\delta\Delta\sigma/\delta D$ is computed by means of a bootstrap approach[53] by 200 realizations of a random sampling with replacement.

Data availability

The dataset used in this paper is freely available at: https://doi.org/10.5281/zenodo.10975747.

Code availability

The code used in this paper is freely available at: https://doi.org/10.5281/zenodo.10975747.

Received: 19 July 2023; Accepted: 17 May 2024;
Published online: 31 May 2024

References

1. Ben-Zion, Y. A Critical Data Gap in Earthquake Physics. *Seismological Res Lett.* **90**, https://doi.org/10.1785/0220190167 (2019).
2. Ellsworth, W. L. & Beroza, G. C. Seismic evidence for a seismic nucleation phase. *Science* **268**, 851–855 (1995).
3. Rikitake, T. Earthquake precursors. *Bull. Seismological Soc. Am.* **65**, 1133–1162 (1975).
4. Jones, L. M. & Molnar, P. Some characteristics of foreshocks and their possible relationship to earthquake prediction and premonitory slip on faults. *J. Geophys. Res.* **84**, 3596–3608 (1979).
5. Abercrombie, R. E. & Mori, J. Occurrence patterns of foreshocks to large earthquakes in the western United States. *Nature* **381**, 303–307 (1996).
6. Dodge, D. A., Beroza, G. C. & Ellsworth, W. L. Detailed observations of California foreshock sequences: Implications for the earthquake initiation process. *J. Geophys. Res.* **101**, 22371–22392 (1996).
7. Kato, A. & Ben-Zion, Y. The generation of large earthquakes. *Nat. Rev. Earth Environ.* **2**, 26–39 (2020).
8. Ben-Zion, Y., Zaliapin, I. Localization and coalescence of seismicity before large earthquakes. *Geophys. J. Int.* **223**, 561–583 (2020).
9. Dresen, G., Kwiatek, G., Goebel, T. & Ben-Zion, Y. Seismic and Aseismic Preparatory Processes Before Large Stick–Slip Failure. *Pure Appl Geophys* **177**, 5741–5760 (2020).
10. Rouet-Leduc, B. et al. Machine Learning Predicts Laboratory Earthquakes. *Geophys Res. Lett.* **44**, 9276–9282 (2017).
11. Karimpouli, S. et al. Explainable machine learning for labquake prediction using catalog-driven features. *Earth Planet. Sci. Lett.* **622**, 118383 (2023).
12. Cotton, F., Archuleta, R. & Causse, M. What is sigma of the stress drop? Seismol. *Res. Lett.* **84**, 42–48 (2013).
13. Picozzi, M. et al. Detecting long-lasting transients of earthquake activity on a fault system by monitoring apparent stress, ground motion and clustering. *Sci. Rep.* **9**, 16268 (2019a).
14. Picozzi, M. et al. Spatiotemporal Evolution of Ground-Motion Intensity at the Irpinia Near-Fault Observatory, Southern Italy. *Bull. Seismological Soc. Am.* **112**, 243–261 (2021a).
15. Picozzi, M., Serlenga, V. & Stabile, T. A. Spatio-temporal evolution of ground motion intensity caused by reservoir-induced seismicity at the Pertusillo artificial lake (southern Italy). *Front. Earth Sci.* **10**, 1048196 (2022).
16. Al Atik, L. et al. The variability of ground-motion prediction models and its components. *Seismol. Res. Lett.* **81**, 794–801 (2010).
17. Causse, M. & Song, S. G. Are stress drop and rupture velocity of earthquakes independent? Insight from observed ground motion variability. *Geophys. Res. Lett.* **42**, 7383–7389 (2015).
18. Bindi, D., Spallarossa, D. & Pacor, F. Between-event and between-station variability observed in the Fourier and response spectra domains: comparison with seismological models. *Geophys. J. Int.* **210**, 1092–1104 (2017).
19. Yu, H. et al. Well proximity governing stress drop variation and seismic attenuation associated with hydraulic fracturing induced earthquakes. *J. Geophys. Res. Solid Earth* **125**, e2020JB020103 (2020).
20. Bindi, D., Cotton, F., Spallarossa, D., Picozzi, M. & Rivalta, E. Temporal Variability of Ground Shaking and Stress Drop in Central Italy: A Hint for Fault Healing? *Bull. Seismological Soc. Am.* **108**, 1853–1863 (2018).
21. Socquet, A. et al. An 8 month slow slip event triggers progressive nucleation of the 2014 Chile megathrust. *Geophys. Res. Lett.* **44**, 4046–4053 (2017).
22. Piña-Valdés, J., Socquet, A., Cotton, F. Insights on the Japanese Subduction Megathrust Properties From Depth and Lateral Variability of Observed Ground Motions. *J. Geophys. Res.*, **123**, 8937–8956 (2018).
23. Piña-Valdés, J., Socquet, A. & Cotton, F. Insights on the Japanese subduction megathrust properties from depth and lateral variability of observed ground motions. *J. Geophys. Res. Solid Earth* **123**, 8937–8956 (2018b).
24. Spallarossa, D., Kotha, S. R., Picozzi, M., Barani, S. & Bindi, D. On-site Earthquake Early Warning: a partially non-ergodic perspective from the site effects point of view. *Geophys. J. Int.* **216**, 919–934 (2019).
25. Iaccarino, A. G., Picozzi, M., Bindi, D. & Spallarossa, D. Onsite earthquake early warning: Predictive models for acceleration response spectra considering site effects. *Bull. Seismological Soc. Am.* **110**, 1289–1304 (2020).
26. Lior, I. & Ziv, A. The relation between ground motion, earthquake source parameters, and attenuation: Implications for source parameter inversion and ground motion prediction equations. *J. Geophys. Res. Solid Earth* **123**, 5886–5901 (2018).

27. Gentili, S., Di Giovambattista, R. & Peresan, A. Seismic quiescence preceding the 2016 central Italy earthquakes. *Phys. Earth Planet. Inter.* **V. 272**, 27–33 (2017).
28. Spallarossa, D. et al. The RAMONES Service for Rapid Assessment of Seismic Moment and Radiated Energy in Central Italy: Concepts, Capabilities, and Future Perspectives. *Seismological Res. Lett.* **92**, 1759–1772 (2021).
29. Waldhauser, F., Michele, M., Chiaraluce, L., Di Stefano, R. & Schaff, D. P. Fault planes, fault zone structure and detachment fragmentation resolved with high- precision aftershock locations of the 2016–2017 central Italy sequence. *Geophys. Res. Lett.* **48**, e2021GL092918 (2021).
30. Vuan, A., Sugan, M., Chiaraluce, L., & Di Stefano, R. Loading rate variations along a mid-crustal shear zone preceding the Mw 6.0 earthquake of 24 August 2016 in Central Italy. *Geophys. Res. Lett.*, **44**, https://doi.org/10.1002/2017GL076223 (2017).
31. Picozzi, M., Spallarossa, D., Bindi, D., Iaccarino, A. G. & Rivalta, E. Detection of spatial and temporal stress changes during the 2016 central Italy seismic sequence by monitoring the evolution of the energy index. *J. Geophys. Res. Solid Earth* **127**, e2022JB025100 (2022).
32. Pino, N. A., Convertito, V. & Madariaga, R. Clock advance and magnitude limitation through fault interaction: the case of the 2016 central Italy earthquake sequence. *Sci. Rep.* **9**, 5005 (2019).
33. Sugan, M., Kato, A., Miyake, H., Nakagawa, S. & Vuan, A. The preparatory phase of the 2009 Mw 6.3 L'Aquila earthquake by improving the detection capability of low-magnitude foreshocks. *Geophys. Res. Lett.* **41**, 6137–6144 (2014).
34. Vičič, B., Aoudia, A., Borghi, A., Momeni, S. & Vuan, A. Seismicity rate changes and geodetic transients in Central Apennines. *Geophys. Res. Lett.* **47**, e2020GL090668 (2020).
35. Malagnini, L. et al. Crustal permeability changes inferred from seismic attenuation: Impacts on multi-mainshock sequences. *Front. Earth Sci.* **10**, 963689 (2022).
36. Mignan, A. Seismicity precursors to large earthquakes unified in a stress accumulation framework. *Geophys. Res. Lett.* **39**, L21308 (2012).
37. Cattania, C. & Segall, P. Precursory Slow Slip and Foreshocks on Rough Faults. *J. Geophys. Res. Solid Earth* **126**, e2020JB020430 (2021).
38. Chiarabba, C. & Chiodini, G. (2013) Continental delamination and mantle dynamics drive topography, extension and fluid discharge in the Apennines. *Geology* **41**, 715–718 (2013).
39. Chiodini, G. et al. Correlation between tectonic CO2 earth degassing and seismicity is revealed by a 10-year record in the Apennines, Italy. *Sci. Adv.* https://doi.org/10.1126/SCIADV.ABC2938/SUPPL_FILE/ABC2938_SM.PDF (2020).
40. Miller, S. A. et al. Aftershocks driven by a high-pressure CO2 source at depth. *Nature* **427**, 724–727 (2004).
41. Collettini, C., Barchi, M. R., de Paola, N., Trippetta, F. & Tinti, E. Rock and fault rheology explain differences between on fault and distributed seismicity. *Nat. Commun.* **13**, 1–11 (2022).
42. Seeber, L. & Armbruster, J. G. Earthquakes as beacons of stress change. *Nature* **407**, 69–72 (2000).
43. Gentili, S., Di Giovambattista, R. Forecasting strong aftershocks in earthquake clusters from northeastern Italy and western Slovenia. *Phys. Earth Planet. Interiors*, **303**, 106483, (2020).
44. Scafidi, D., Spallarossa, D., Turino, C., Ferretti, G. & Viganò, A. Automatic P- and S-wave local earthquake tomography: testing performance of the automatic phase-picker engine "RSNI-Picker". *Bull. Seismol. Soc. Am.* **106**, 526–536 (2016).
45. Spallarossa, D., Ferretti, G., Scafidi, D., Turino, C. & Pasta, M. Performance of the RSNI-Picker. *Seismol. Res. Lett.* **85**, 1243–1254 (2014).
46. Spallarossa, D. et al. An automatically generated high-res- olution seismic catalogue for the 2016–2017 Central Italy sequence, including P and S phase arrival times. *Geophys. J. Int.* **225**, 555–571 (2021).
47. Bindi, D., Parolai, S., Grosser, H., Milkereit, C. & Durukal, E. Empirical ground-motion prediction equations for northwestern Turkey using the aftershocks of the 1999 Kocaeli earthquake. *Geophys. Res. Lett.* **34**, L08305 (2007).
48. Bates, D., Maechler, M., Bolker, B. & Walker, S. Fitting linear mixed-effects models using lme4. *J. Stat. Softw.* **67**, 1–48, (2015).
49. Zaliapin, I. & Ben-Zion, Y. Discriminating characteristics of tectonic and human-induced seismicity. *Bull. Seismological Soc. Am.* **106**, 846–859 (2016).
50. Bindi, D., Picozzi, M., Spallarossa, D., Cotton, F. & Kotha, S. R. Impact of Magnitude Selection on Aleatory Variability Associated with Ground-Motion Prediction Equations: Part II—Analysis of the Between-Event Distribution in Central Italy. *Bull. Seismological Soc. Am.* **109**, 251–262 (2019).
51. Kotha, S. R., Bindi, D. & Cotton, F. From Ergodic to Region- and Site-Specific Probabilistic Seismic Hazard Assessment: Method Development and Application at European and Middle Eastern Sites. *Earthquake Spectra*, **33**, 1433–1453 (2017).
52. Kotha, S. R., Weatherill, G., Bindi, D. & Cotton, F. A regionally adaptable ground motion model for shallow crustal earthquakes in 818 Europe. *Bull. Earth Eng.* **18**, 4091–4125 (2020).
53. Efron, B. Bootstrap methods: another look at the jackknife. *Ann. Stat.* **7**, 1–26 (1979).
54. Anderson, J. G. & Hough, S. E. A model for the shape of the Fourier amplitude spectrum of acceleration at high frequencies. *Bull. Seismological Soc. Am.* **74**, 1969–1993 (1984).
55. Brune, J. N. Tectonic stress and the spectra of seismic shear waves from earthquakes. *J. Geophys. Res.* **75**, 4997–5009 (1970).
56. Madariaga, R. Dynamics of an expanding circular fault. *Bull. Seismol. Soc. Am.* **66**, 639–666 (1976).
57. Gutenberg, B. & Richter, C. F. Earthquake magnitude, intensity, energy, and acceleration. *Bull. Seismol. Soc. Am.* **46**, 105–145 (1956).
58. Malagnini, L., Lucente, F. P., De Gori, P., Akinci, A. & Munafo', I. Control of pore fluid pressure diffusion on fault failure mode: Insights from the 2009 L'Aquila seismic sequence. *J. Geophys. Res.* **117**, B05302 (2012).
59. Luzi, L. et al. The central Italy seismic sequence between August and Decem- ber 2016: Analysis of strong-motion observations. *Seismological Res. Lett.* **88**, 1219–1231 (2017).

Acknowledgements

We thank Luca Dal Zilio and three anonymous reviewer for providing insightful comments and suggestions which greatly improve the value of this work. This research was supported by the PRIN 2022 project '2022ZHXWC9'—Intercepting the PREparatory Phase of lARge earthquakes from seismic information and gEodetic Displacement (PREPARED), and the Program STAR PLUS (project DRAGON), financially supported by UniNA and Compagnia di San Paolo.

Author contributions

D.S. prepared the datasets. M.P. and D.S. conducted the analysis. M.P., D.S., A.G.I. and D.B. jointly analyzed and interpreted the results and wrote the manuscript.

Competing interests
The authors declare no competing interests.

Additional information
Supplementary information The online version contains supplementary material available at https://doi.org/10.1038/s43247-024-01455-y.

Correspondence and requests for materials should be addressed to Matteo Picozzi.

Peer review information *Communications Earth & Environment* thanks Milad Kowsari and the other, anonymous, reviewer(s) for their contribution to the peer review of this work. Primary Handling Editors: Luca Dal Zilio and Joe Aslin. A peer review file is available